JOURNAL OF
EMERGING INVESTIGATORS

Article

Advancements in glioma segmentation: comparing the U-Net and DeconvNet models

Amaan A. Mohammed[1], Ricardo A. Gonzales[2]

[1] Dublin High School, Dublin, California

[2] Radcliffe Department of Medicine, University of Oxford, Oxford, United Kingdom

SUMMARY

In this study, we address the challenge of accurately segmenting gliomas from magnetic resonance imaging (MRI) scans, an essential task for treatment planning and prognosis in glioma patients. Prompted by the limitations of manual segmentation methods and the need for precise automated techniques, we evaluated the efficacy of advanced deep learning models in this domain. Our primary objective was to compare the performance of two convolutional neural network architectures, the U-Net and a baseline DeconvNet model, in segmenting (outlining) gliomas from surrounding tissues in MRI scans. We hypothesized that the U-Net model would outperform the DeconvNet model in segmenting tumors due to U-Net's advanced architecture (skip connections). Utilizing the Multimodal Brain Tumor Image Segmentation (BraTS) 2018 dataset for training and validation, we evaluated the models based on the Dice Similarity Coefficient (DSC) to quantify segmentation accuracy. We found that the U-Net model achieved a significantly higher average DSC of 0.918 ± 0.053, compared to 0.867 ± 0.065 for DeconvNet model ($p < 0.05$), indicating superior accuracy in tumor delineation. Furthermore, the U-Net model showed more stable training and validation losses, suggesting better adaptability to new data. We concluded that the U-Net model's advanced capabilities enhanced glioma segmentation in MRI scans, surpassing the baseline DeconvNet method. Our findings may help improve non-invasive diagnostic procedures and treatment planning in glioma patients, reinforcing the value of integrating advanced neural network architectures into medical imaging.

INTRODUCTION

Gliomas are a prevalent form of brain tumor originating from glial cells, a diverse group of cell types that support the growth, maintenance, and repair of the nervous system (1). One type of glial cell, oligodendrocytes, produces the myelin sheath of axons to facilitate rapid signaling (1). Other glial cells, including astrocytes, ependymal cells, and microglia, also play a broader role in brain function and pathology. Overgrowth of these cells can lead to the advancement of glioma formation (1). Gliomas originate from the overgrowth of these glial cells, which clump to form a tumor mass. The prognosis for patients diagnosed with high-grade gliomas is particularly dire, with survival rates dropping pronouncedly within two years of diagnosis (2). Immediate and effective treatment is critical for these patients, as gliomas can rapidly grow into higher grades and exert pressure on the brain, which can impair normal function and lead to brain damage (3). Historical data indicates that patients with Grade I glioma have a five-year survival close to 95%, as opposed to Grade III and Grade IV, which have a less than a 30% chance and less than a 10% chance of survival, respectively (4). Therefore, without proper monitoring or early diagnosis of glioma, a cure becomes much less likely.

Glioma remains the most common malignant primary intracranial tumor, accounting for 81% of such tumors, and is the most common form of central nervous system neoplasm originating from glial cells (5). In the United States, approximately 6 out of every 100,000 people are diagnosed with gliomas every year (5). The current standard-of-care treatment includes maximal surgical resection, postoperative concurrent chemoradiotherapy, and maintenance chemotherapy (6). Even with clinical trials to further improve treatment outcomes, the median survival rate for glioblastoma (Grade IV glioma) remains low at approximately 14 to 20 months (7).

Advancements in neuroimaging have played a crucial role in the detection and analysis of gliomas. Magnetic resonance imaging (MRI) provides detailed, non-invasive views of the brain, enabling clinicians to assess key tumor characteristics like size, shape, and localization. MRI modalities, including parametric mapping, are particularly effective in highlighting variations in tissue properties surrounding tumors. Native T1 MRI scans offer a clear contrast between different brain tissues, which is vital for accurately delineating gliomas (8). These imaging modalities aid planning treatments, such as radiation therapy, by providing a comprehensive understanding of the tumor's anatomy.

Despite the detailed imaging provided by MRI, accurately segmenting the tumor from healthy brain tissue remains challenging. Radiologists are tasked with manual segmentation, a process that involves outlining the tumor's boundaries on an MRI by drawing the tumor's extent pixel by pixel to separate it from surrounding healthy tissue. The radiologists visually differentiate the tumor characteristics through MRI sequences, which show subtle intensity differences between tumor and healthy tissue (6). This procedure is not only time-consuming but also highly dependent on the radiologist's expertise and subjective judgment (9). The variability inherent in manual segmentation can lead to inconsistent and suboptimal treatment outcomes (9). Additionally, the diverse nature of gliomas, with variations in size, extension, and location across patients, complicates the use of standard segmentation algorithms (10).

https://doi.org/10.59720/24-022

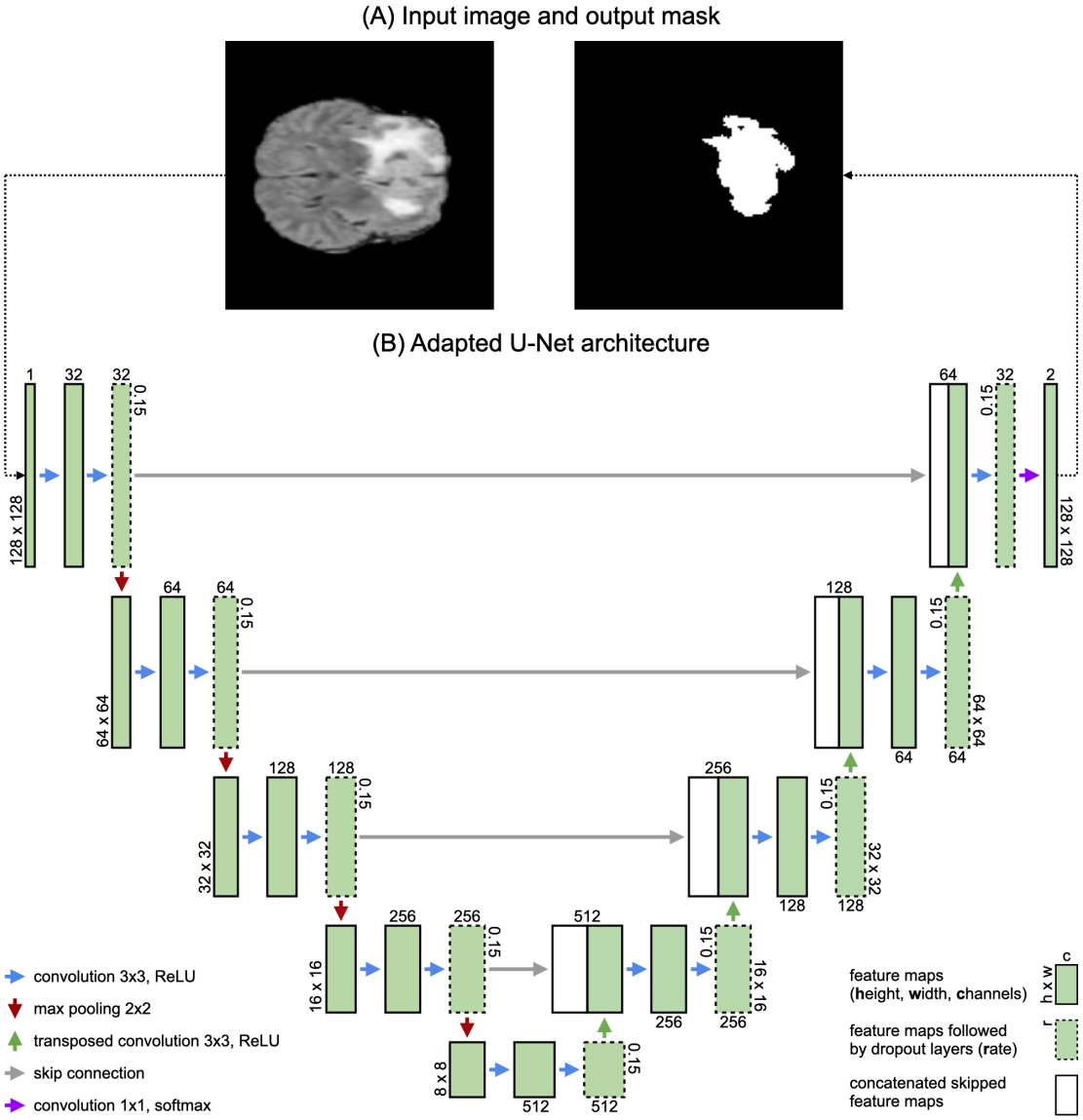

Figure 1: U-Net architecture for brain tumor segmentation from MRI scans. (A) Input MRI scan and the corresponding output segmentation mask, illustrating the tumor area. (B) Adapted U-Net architecture utilized for tumor segmentation, showing the flow from input image to output mask through the network's layers, including convolutional layers, max pooling, transposed convolutions, and skip connections that facilitate feature map concatenation (13).

In response to these challenges, computational models have been developed to automate the tumor segmentation process. Convolutional neural networks (CNNs) with encoder-decoder architectures have emerged as a promising tool for this task (11). These models process MRI scans to detect and segment brain tumors, reducing the reliance on manual methods. Among the various CNN architectures, the standard encoder-decoder architecture, known as DeconvNet, and the U-Net model have gained attention for their effectiveness in image segmentation (12). These models are particularly suited for tasks with limited training data and are designed to provide precise segmentations by adding consecutive layers that enhance the resolution of the output (13).

The DeconvNet and U-Net models share similarities in their structure but differ considerably in their approach to segmentation. The DeconvNet model consists of a sequence of convolutional and pooling layers to encode the input into a compressed representation, followed by a series of upsampling layers to decode this representation back into an image (13). In contrast, the U-Net model incorporates skip connections that link corresponding layers in the encoder and decoder paths. These connections allow the U-Net to retain high-resolution features from the input image, enabling more precise segmentations (14). The incorporation of these skip connections facilitates efficient learning in deeper network layers by mitigating the vanishing gradient problem, an issue that arises when gradients diminish as they are backpropagated through layers in a neural network, causing early layers to learn very slowly or not at all (15, 16).

Previous research has explored the applications of U-Net and DeconvNet in various image segmentation tasks (17-19). Studies comparing these models, such as in urban scene segmentation using the CityScapes dataset, have demonstrated that both architectures are effective

https://doi.org/10.59720/24-022

but may perform differently depending on the task (17). For example, U-Net's skip connections can enable more precise segmentation, while DeconvNet's structure can be advantageous in contexts where capturing high-level features and maintaining spatial resolution during upsampling are critical, such as in scenarios with large-scale object segmentation or when working with lower-resolution images (17). Additionally, research in remote sensing has explored hybrid models combining elements of U-Net and DeconvNet to enhance segmentation accuracy and efficiency, showcasing the potential for these architectures to be used synergistically (18). Moreover, U-Net has been further developed with multi-scale and residual convolutions, leading to superior performance in segmenting complex structures like retinal vessels (19). These studies highlight the versatility of both models and underscore the need for further comparison. We aimed to build on these findings by directly comparing U-Net and DeconvNet in segmenting gliomas from MRI scans.

Several studies have successfully applied U-Net-based frameworks to brain tumor segmentation, particularly gliomas, further emphasizing its relevance in this context. For instance, a U-Net-based system for segmenting gliomas from FLAIR MRI sequences and predicting biomarkers such as IDH-1 and MGMT achieved a high segmentation accuracy, measured by Dice Similarity Coefficient (DSC), of 0.93 (20). Similarly, an improved U-Net design with hybrid dilated convolutions showed high performance in capturing tumor boundary details and edge precision in segmentation tasks (21). A 3D U-Net model implemented on the BraTS dataset using a cloud-based architecture achieved state-of-the-art segmentation accuracy with a DSC of 0.95 (22). Despite these successes, a one-to-one comparison between the U-Net and DeconvNet architectures in glioma segmentation is lacking, leaving a critical gap in understanding whether U-Net's advanced architectural features, particularly skip connections, consistently lead to superior performance in this medical domain. Our work aims to address this gap while building on existing U-Net advancements.

We hypothesized that the U-Net model, with its advanced architecture, would outperform the traditional DeconvNet model in segmenting gliomas from MRI scans. To test this hypothesis, we applied both models to the BraTS 2018 dataset and compared their segmentation accuracy using the DSC. Our findings demonstrated that U-Net outperformed DeconvNet in accurately delineating tumor boundaries. This advancement suggests an improvement in the non-invasive diagnosis and treatment planning for glioma patients. Automating the segmentation process could contribute to early diagnosis by enabling the detection of low-grade tumors, facilitating rapid and efficient screening, and reducing the need for extensive human labor. Our study highlights U-Net's advanced capabilities in glioma segmentation and its potential real-world clinical impact in improving diagnostic precision and patient outcomes.

RESULTS

We trained and compared two neural network models to segment brain tumors in MRI scans into two major classes: the tumor and the background (**Figure 1A**). From the Multimodal Brain Tumor Image Segmentation (BraTS) 2018 dataset, a comprehensive collection of MRI scans from 285 patients with low-grade and high-grade gliomas, we used the available 4715 native T1-weighted images (10). The dataset was partitioned into training, with 3756 images (80%), and validation, with 959 images (20%). This provides a sufficiently large dataset for training to optimize learning while reserving a meaningful portion for unbiased evaluation of the model's performance on unseen data. The input image was the initial MRI scan showing the brain with white differentiations in the left and right frontal lobes, indicating the location of gliomas. The output image displayed the segmentation of the tumor, with white space representing the tumor outline and the background, with black space representing non-tumor brain tissue and other miscellaneous signals. Our simpler model used a baseline encoder-decoder architecture, or DeconvNet, which processed the input

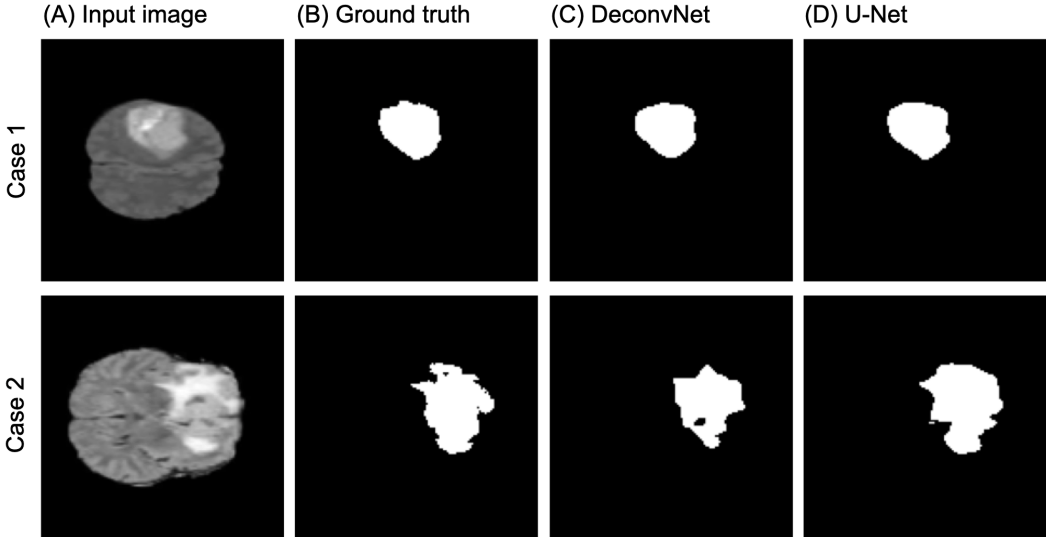

Figure 2: Segmentation examples for the DeconvNet and U-Net models. Two examples are provided, with each row consisting of (A) an MRI from a glioma patient, (B) the actual depiction of the mask by an expert radiologist from the BraTS 2018 dataset (10), (C) the mask predicted by the DeconvNet model, and (D) the mask predicted by the U-Net model.

https://doi.org/10.59720/24-022

image through successive convolutional and pooling layers before reconstructing the segmented output. The other, more advanced U-Net architecture incorporated skip connections that link corresponding layers in the encoder and decoder paths, enabling the model to retain high-resolution features for more precise segmentation (14) (**Figure 1B**). Both models were trained using the same dataset, consisting of MRI scans from the BraTS 2018 dataset (10). The primary metric for evaluating model performance was the Dice Similarity Coefficient (DSC), which quantitatively assessed the accuracy of the model's segmentation against the actual tumor outlines in the MRI scans, also referred to as the ground truth mask (23). The closer the DSC was to 1.0, the higher the accuracy of the model's segmentation.

We examined side-by-side comparisons of the input image, ground truth mask, and the predicted masks from both the baseline and U-Net models (**Figure 2**). We observed that the U-Net had more precise tumor boundary delineation than the DeconvNet, as the tumor outline of the ground truth mask closely resembled the U-Net, while the DeconvNet did not capture an accurate delineation. More specifically, for the first case, the DSCs were 0.963 and 0.971 for the DeconvNet and the U-Net models, respectively; similarly, for the second case, the DSCs were 0.840 and 0.905. The distribution of DSC values indicated a more favorable outcome for the U-Net model (**Figure 3**). Specifically, on the validation set (n = 959), the U-Net model achieved a higher average DSC (mean ± standard deviation) of 0.918 ± 0.053 (median: 0.930), compared to the DeconvNet model's DSC of 0.867 ± 0.065 (median: 0.880). In the cross-validation experiment, the standard deviation across folds, which measures the variability of model performance across different subsets of the data, was low for both U-Net (0.015) and DeconvNet (0.021), ensuring the results were consistent even if another subset was chosen for evaluation purposes. In each fold, the DSCs of the U-Net model were significantly higher than the DeconvNet's performance ($p < 0.05$), confirming that the U-Net model provided more accurate segmentations of brain tumors.

The training curves for both models revealed distinct patterns of loss (**Figure 4A**). The DeconvNet model exhibited an increase in validation loss, which may be indicative of overfitting. Overfitting occurs when a model learns the details and noise in the training data to the extent that it negatively impacts the model's performance on new data (24). Conversely, the validation loss for the U-Net model remained stable, suggesting a better generalization to unseen data. While the loss curves indicate overfitting due to the imbalanced class distribution (with many more background pixels), the DSC metric curve specifically measures the performance of glioma segmentation. While both models showed stable DSC metric curves, the U-Net model consistently outperformed the baseline model, reinforcing its effectiveness in brain tumor segmentation tasks (**Figure 4B**). These results highlight the advanced capabilities of the U-Net architecture in accurately segmenting gliomas from MRI scans, compared to the traditional DeconvNet model.

DISCUSSION

Our research evaluated the performance of U-Net and DeconvNet models in segmenting MRI scans of glioma patients, hypothesizing that U-Net would outperform

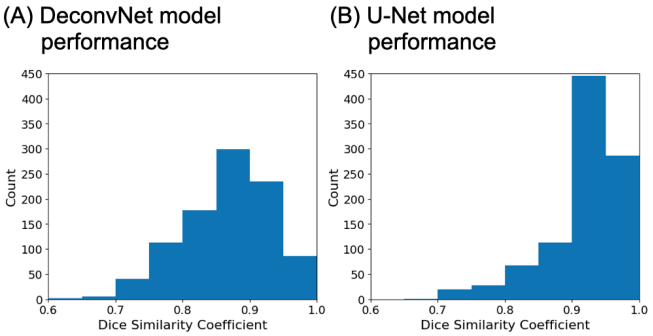

Figure 3: Comparative performance by Dice Similarity Coefficient of the DeconvNet and U-Net models. Histograms comparing the distribution of Dice Similarity Coefficient (DSC) scores (n = 959) for the (A) baseline (DeconvNet) and (B) advanced (U-Net) models. The DSC scores reflect the accuracy of tumor segmentation in each MRI scan, with the count of occurrences plotted against 0.05 DSC score intervals.

DeconvNet in segmentation accuracy. The U-Net model achieved a DSC of 0.904 ± 0.046 on the validation set (n = 959) and maintained stable training and validation losses, demonstrating its ability to segment gliomas of various sizes and locations. The skip connections in the U-Net architecture addressed the vanishing gradient problem and enabled effective learning in deeper network layers, resulting in more accurate segmentation compared to DeconvNet. These results highlight the potential of U-Net for improving segmentation tasks in medical imaging.

Our results are consistent with previous studies demonstrating the superior performance of U-Net in brain tumor segmentation tasks, further validating its role as a reliable model in medical imaging applications. For example, a DSC of 0.93 was achieved with an improved U-Net design incorporating hybrid dilated convolutions, and a DSC of 0.95 was delivered by a 3D U-Net on the BraTS dataset (21, 22). Both results closely align with our DSC of 0.918 ± 0.053, though the slight differences in performance may be attributed to factors such as the inclusion of additional MRI modalities, 3D extensions, or architectural enhancements like hybrid convolutions, which were not used in our study (21, 22). Despite this, our findings uniquely highlight the performance difference between U-Net and DeconvNet in the context of glioma segmentation, where U-Net significantly outperformed DeconvNet (DSC of 0.918 vs. 0.867, $p < 0.05$). This gap in performance is largely due to U-Net's skip connections, which preserve high-resolution spatial features during upsampling and improve learning efficiency by addressing the vanishing gradient problem (15, 16). Moreover, U-Net's ability to retain multi-scale features and capture fine-grained tumor boundaries enables better segmentation accuracy, particularly for irregularly shaped or small lesions, which DeconvNet struggles to capture due to its lack of feature-preserving skip connections.

Despite these promising outcomes, it is important to recognize the limitations of the study. The reliance on the BraTS 2018 dataset may present certain constraints due to its specific composition, such as a relatively limited number of cases, potential selection bias, and variations in imaging

https://doi.org/10.59720/24-022

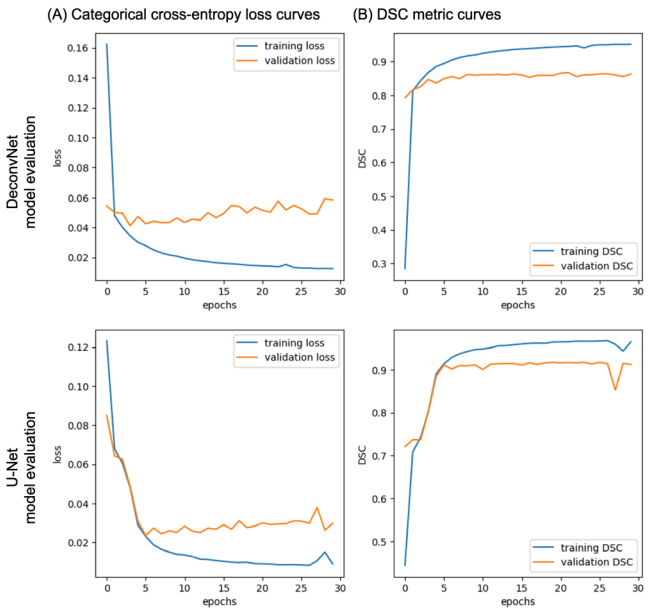

Figure 4: Loss and performance curves for the DeconvNet and U-Net models during training. (A) Categorical cross-entropy loss curves and (B) Dice Similarity Coefficient (DSC) metric for the DeconvNet model (top) and the U-Net model (bottom), comparing training and validation loss across epochs.

protocols across contributing institutions. Additionally, the focus on a single MRI sequence, native T1 maps, restricts the breadth of the findings, as it excludes valuable information that could be gleaned from other sequences like T2-weighted, FLAIR, and contrast-enhanced T1-weighted images. These other sequences are also available in the BraTS 2018 dataset, and each provides unique insights: T2-weighted images are particularly effective in highlighting edema, FLAIR sequences are useful for detecting lesions and abnormal fluid accumulations, and contrast-enhanced T1-weighted images can reveal areas of active tumor growth by highlighting regions with disrupted blood-brain barriers (25). By relying solely on native T1 maps, the study may miss critical information about tumor heterogeneity, edema, and necrotic regions that are essential for a comprehensive analysis of gliomas. These limitations highlight areas for further research, including the integration of multiple MRI sequences and a more diverse dataset to enhance the robustness and generalizability of the findings.

Future research should aim to broaden the scope of the dataset by incorporating multiple MRI sequences to enhance the robustness of the findings. Exploring emerging neural network architectures, such as vision transformers, could provide new avenues for advancement in medical image segmentation (26). Additionally, including a wider array of tumor classes could potentially improve the generalizability of the models, making them more versatile in clinical applications. The models can also be trained on different datasets that each contain one type of tumor to determine if the U-Net model performs better with specific types of tumors.

Both U-Net and DeconvNet exemplify the transformative role of AI in healthcare by automating tumor segmentation, improving diagnostic accuracy, reducing clinician workload, and enhancing patient care. The integration of AI in healthcare, particularly for diagnosing and treating gliomas, requires certain ethical considerations. Ensuring patient privacy and data security is critical given the sensitive nature of medical information and the increasing risk of data breaches (27). Addressing potential biases in AI algorithms is also essential, as imbalances in training datasets can lead to disparities in treatment outcomes, potentially exacerbating existing health inequities (28). Moreover, transparency in AI decision-making processes and maintaining clear human oversight are vital to upholding trust and accountability in clinical settings (28). By considering these ethical aspects, the responsible use of AI can be better integrated into healthcare, ensuring both technological advancement and patient welfare.

In conclusion, we have effectively demonstrated the superiority of the U-Net convolutional neural network in segmenting gliomas from MRI scans over the traditional DeconvNet model. These results contribute to the growing body of research advocating for the use of advanced neural network architectures in medical imaging. The identified limitations and suggested future research directions underscore the ongoing need for refinement and evolution of these models with the aim of enhancing their clinical applicability and efficacy.

MATERIALS AND METHODS

Imaging Dataset

The study utilized the BraTS 2018 dataset, retrospectively acquired at Bern University (Bern, Switzerland), Debrecen University (Debrecen, Hungary), Heidelberg University (Heidelberg, Germany), and Massachusetts General Hospital (Boston, United States) (10). The dataset included manual tumor delineations by expert radiologists. For this research, we used native T1 maps from the dataset due to their non-invasive nature. This selection allowed for a detailed analysis of brain tissue and tumor structure without the need for invasive contrast agents.

Data Preprocessing

The MRI scans were converted into JPEG files and stored in a Google Drive folder for accessibility and ease of data handling. Utilizing Google Colab, a cloud-based Integrated Development Environment, the Python Imaging Library and other necessary libraries were employed for image processing (29).

U-Net Architecture

We used the U-Net model given its efficacy in medical image segmentation (14). U-Net is characterized by its unique structure resembling the letter “U” (14). It comprises two primary components: a contracting path to capture context and an expansive path that enables precise localization. The contracting path consists of repeated application of convolutions and pooling operations, while the expansive path involves upsampling operations and convolutions (30). Each of the four levels in the contracting and expansive paths is skip-connected (**Figure 1B**). Skip connections provide shortcut paths for gradients to flow directly from deeper layers to shallow layers, helping to mitigate the vanishing gradient problems (31). U-Net’s design allows for the detailed segmentation of images, capturing fine details that are crucial for accurate tumor delineation.

https://doi.org/10.59720/24-022

DeconvNet Architecture

In contrast to the U-Net model, we employed a standard encoder-decoder architecture as the baseline model. This architecture is similar to the U-Net in its overall design but lacks the skip connections and concatenations that are characteristic of the U-Net. The DeconvNet model relies on a sequence of convolutional and pooling layers to encode the input into a feature-rich, compressed representation (12). The decoder then reconstructs the image from this encoded representation. The absence of skip connections means that this model may not capture fine details as effectively as the U-Net model.

Model Hyperparameters and Optimization

Both the U-Net and DeconvNet were trained on Tensorflow using identical hyperparameters to ensure a fair comparison (32). The training involved a batch size of 16 images (meaning 16 images were processed in each iteration) and a total of 30 epochs to allow the models sufficient learning time (33). The Adam optimizer, known for its effectiveness in handling sparse gradients on noisy problems, was used for weight adjustments during training (34). The loss function used was categorical cross-entropy, which measures the performance of the model in segmenting the different classes in the images and is a standard choice for segmentation problems. The best model weights, corresponding to the epoch with the highest validation Dice accuracy, were saved and chosen during training. The code for preprocessing the data and for training and evaluating the models is accessible in the following repository: https://github.com/AmaanDublin/U-Net.

Model Evaluation and Statistical Analysis

For model evaluation, our primary metric was the DSC, a statistical tool used to gauge the similarity between two samples (22). The metric measures how closely the predicted segmentation of the models aligns with the actual, manually delineated tumor segments in the MRI scans. The DSC values were reported as mean ± standard deviation (median). A five-fold cross-validation with homogeneous distribution was performed for both models to avoid bias in the selection of the validation set. For statistical analysis, a paired t-test was conducted on the DSCs from the validation set, comparing the results between the DeconvNet and U-Net models (36).

ACKNOWLEDGMENTS

We would like to acknowledge mentorship support from Veritas AI.

Received: January 16, 2024
Accepted: August 31, 2024
Published: May 29, 2025

REFERENCES

1. Jäkel, Sarah, and Leda Dimou. "Glial Cells and Their Function in the Adult Brain: A Journey through the History of Their Ablation." *Frontiers in Cellular Neuroscience*, vol. 11, no. 24, Feb. 2017, pp. 1-17, https://doi.org/10.3389/fncel.2017.00024.
2. Ghotme, Kemel A., et al. "Gliomas: New Perspectives in Diagnosis, Treatment and Prognosis." *Current Topics in Medicinal Chemistry*, vol. 17, no. 12, Mar. 2017, pp. 1438–1447, https://doi.org/10.2174/1568026617666170103162639.
3. Enam, Syed Faaiz, et al. "Cytostatic Hypothermia and Its Impact on Glioblastoma and Survival." *Science Advances*, vol. 8, no. 47, Nov. 2022, https://doi.org/10.1126/sciadv.abq4882.
4. Weller, Michael, et al. "Glioma." *Nature Reviews. Disease Primers*, vol. 1, no. 1, 2015, p. 15017, https://doi.org/10.1038/nrdp.2015.17.
5. Davis, Mary Elizabeth. "Epidemiology and Overview of Gliomas." *Seminars in Oncology Nursing*, vol. 34, no. 5, Dec. 2018, pp. 420–429, https://doi.org/10.1016/j.soncn.2018.10.001.
6. Kotecha, Rupesh, et al. "Key Clinical Principles in the Management of Glioblastoma." *JCO Oncology Practice*, vol. 19, no. 4, Apr. 2023, pp. 180–189, https://doi.org/10.1200/op.22.00476.
7. Gilard, Vianney, et al. "Diagnosis and Management of Glioblastoma: A Comprehensive Perspective." *Journal of Personalized Medicine*, vol. 11, no. 4, 1 Apr. 2021, p. 258, https://doi.org/10.3390/jpm11040258.
8. Mikheev, Artem, et al. "Fully Automatic Segmentation of the Brain from T1-Weighted MRI Using Bridge Burner Algorithm." *Journal of Magnetic Resonance Imaging*, vol. 27, no. 6, May 2008, pp. 1235–1241, https://doi.org/10.1002/jmri.21372.
9. Huang, Meiyan, et al. "Brain Tumor Segmentation Based on Local Independent Projection-Based Classification." *IEEE Transactions on Bio-Medical Engineering*, vol. 61, no. 10, Oct. 2014, pp. 2633–2645, https://doi.org/10.1109/TBME.2014.2325410.
10. Menze, Bjoern H., et al. "The Multimodal Brain Tumor Image Segmentation Benchmark (BRATS)." *IEEE Transactions on Medical Imaging*, vol. 34, no. 10, Oct. 2015, pp. 1993–2024, https://doi.org/10.1109/tmi.2014.2377694.
11. Jozwik, Kamila M., et al. "Deep Convolutional Neural Networks Outperform Feature-Based but Not Categorical Models in Explaining Object Similarity Judgments." *Frontiers in Psychology*, vol. 8, Oct. 2017, p. 1721, https://doi.org/10.3389/fpsyg.2017.01726.
12. Noh, Hyeonwoo, et al. "Learning Deconvolution Network for Semantic Segmentation." *Proceedings of the IEEE International Conference on Computer Vision (ICCV)*, edited by Bajcsy, Ruzena, et al., IEEE, Dec 2015, pp. 1520–1528, https://doi.org/10.1109/ICCV.2015.178.
13. Ye, Jong Chul, and Woon Kyoung Sung. "Understanding Geometry of Encoder-Decoder CNNs." *Proceedings of the 36th International Conference on Machine Learning*, edited by Chaudhuri, Kamalika, et al., PLMR, May 2019, pp. 7064-7073. proceedings.mlr.press/v97/ye19a.html.
14. Ronneberger, Olaf, et al. "U-Net: Convolutional Networks for Biomedical Image Segmentation." *Lecture Notes in Computer Science*, edited by Navab, Nassir, et al., Springer, vol. 9351, 2015, pp. 234–241, https://doi.org/10.1007/978-3-319-24574-4_28.
15. Das, Suchsimita, et al. "Effect of Learning Parameters on the Performance of U-Net Model in Segmentation of Brain Tumor." *Multimedia Tools and Applications*, vol. 81, Aug. 2021, pp. 34717–34735, https://doi.org/10.1007/s11042-021-11273-5.
16. Hochreiter, Sepp. "The Vanishing Gradient Problem during Learning Recurrent Neural Nets and Problem Solutions."

https://doi.org/10.59720/24-022

International Journal of Uncertainty, Fuzziness and Knowledge-Based Systems, vol. 06, no. 02, Apr. 1998, pp. 107–116, https://doi.org/10.1142/s0218488598000094.
17. Kothari, Jash Jayesh, et al. "Performance of Deconvolution Network and UNET Network for Image Segmentation." *Smart Innovation, Systems and Technologies*, edited by Bhateja, Vikrant, et al., Springer, Jan. 2022, pp. 361–368, https://doi.org/10.1007/978-981-16-6616-2_34.
18. Su, Zhongbin, et al. "An Improved U-Net Method for the Semantic Segmentation of Remote Sensing Images." *Applied Intelligence*, vol. 52, no. 3, July 2021, pp. 3276–3288, https://doi.org/10.1007/s10489-021-02542-9.
19. Yang, Xin, et al. "MR-UNet: An UNet Model Using Multi-Scale and Residual Convolutions for Retinal Vessel Segmentation." *International Journal of Imaging Systems and Technology*, vol. 32, no. 5, Mar. 2022, pp. 1588–1603, https://doi.org/10.1002/ima.22728.
20. Kihira, Shingo, et al. "U-Net Based Segmentation and Characterization of Gliomas." *Cancers*, vol. 14, no. 18, Sept. 2022, pp. 4457–4457, https://doi.org/10.3390/cancers14184457.
21. Zheng, Ping, et al. "Brain Tumour Segmentation Based on an Improved U-Net." *BMC Medical Imaging*, vol. 22, no. 1, Nov. 2022, p. 199, https://doi.org/10.1186/s12880-022-00931-1.
22. Shaukat, Zeeshan, et al. "A State-of-The-Art Technique to Perform Cloud-Based Semantic Segmentation Using Deep Learning 3D U-Net Architecture." *BMC Bioinformatics*, vol. 23, no. 1, June 2022, p. 251, https://doi.org/10.1186/s12859-022-04794-9.
23. Dice, Lee R. "Measures of the Amount of Ecologic Association between Species." *Ecology*, vol. 26, no. 3, July 1945, pp. 297–302, https://doi.org/10.2307/1932409.
24. Hawkins, Douglas M. "The Problem of Overfitting." *ChemInform*, vol. 35, no. 19, May 2004, https://doi.org/10.1002/chin.200419274.
25. Widmann, Gerlig, et al. "MRI Sequences in Head & Neck Radiology – State of the Art." *Fortschr Röntgenstr*, vol. 189, no. 05, Apr. 2017, pp. 413–422, https://doi.org/10.1055/s-0043-103280.
26. Dosovitskiy, A., et al. "An image is worth 16x16 words: Transformers for image recognition at scale." *9th International Conference on Learning Representations*, edited by Mohamed, Shakir, et al., ICLR, 2021, pp. 1-21.
27. Itai Bavli, et al. "Ethical Concerns around Privacy and Data Security in AI Health Monitoring for Parkinson's Disease: Insights from Patients, Family Members, and Healthcare Professionals." *AI & Society*, vol. 40, Jan. 2024, pp. 155–165, https://doi.org/10.1007/s00146-023-01843-6.
28. Arafa, Ahmed, et al. "Emerging Digital Technologies in Healthcare with a Spotlight on Cybersecurity: A Narrative Review." *Information*, vol. 14, no. 12, Dec. 2023, p. 640, https://doi.org/10.3390/info14120640.
29. Bisong, Ekaba. *Building Machine Learning and Deep Learning Models on Google Cloud Platform: A Comprehensive Guide for Beginners*. New York, Apress, 2019.
30. Minaee, Shervin, et al. "Image Segmentation Using Deep Learning: A Survey." *IEEE Transactions on Pattern Analysis and Machine Intelligence*, vol. 44, no. 7, 2021, pp. 3523-3542, https://doi.org/10.1109/tpami.2021.3059968.
31. Gammell, Jimmy, et al. "Layer-Skipping Connections Improve the Effectiveness of Equilibrium Propagation on Layered Networks." *Frontiers in Computational Neuroscience*, vol. 15, May 2021, p. 627357, https://doi.org/10.3389/fncom.2021.627357.
32. Abadi, Martin, et al. "TensorFlow: A System for Large-Scale Machine Learning." *12th USENIX Symposium on Operating Systems Design and Implementation (OSDI 16)*, edited by Keeton, Kimberly, et al., USENIX Association, 2016, pp. 256-283.
33. Yang, Li, and Abdallah Shami. "On Hyperparameter Optimization of Machine Learning Algorithms: Theory and Practice." *Neurocomputing*, vol. 415, Nov. 2020, pp. 295–316, https://doi.org/10.1016/j.neucom.2020.07.061.
34. Kingma, Diederik P., and Ba, Jimmy. "Adam: A method for stochastic optimization." *3rd International Conference on Learning Representations*, edited by Bengio, Yosua, et al., ICLR, 2015, pp. 1-15, https://doi.org/10.48550/arXiv.1412.6980.
35. Yeung, Michael, et al. "Calibrating the Dice Loss to Handle Neural Network Overconfidence for Biomedical Image Segmentation." *Journal of Digital Imaging*, vol. 36, no. 2, Dec. 2022, pp. 739–752, https://doi.org/10.1007/s10278-022-00735-3.
36. Kalpić, Damir, et al. "Student's T-Tests." *International Encyclopedia of Statistical Science*, edited by Miodrag Lovric, Springer, 2011, pp. 1559–1563, https://doi.org/10.1007/978-3-642-04898-2_641.